Wavefront sensorless adaptive optics based on the trust region method

Qingyun Yang,* Jinyu Zhao, Minghao Wang, and Jianlu Jia

Changchun Institute of Optics, Fine Mechanics and Physics, Chinese Academy of Sciences, Changchun 130033, China
**Corresponding author: qingyunyang77@gmail.com*

Received January 14, 2015; revised February 9, 2015; accepted February 17, 2015;
posted February 18, 2015 (Doc. ID 232332); published March 18, 2015

We present what is to the best of our knowledge the first implementation of a trust region method for derivative-free optimization (TRDF) in a wavefront sensorless (WFSless) adaptive optics (AO) system. We compare the trust region method with the simulated annealing (SA) algorithm and stochastic parallel gradient descent (SPGD) algorithm. The experimental results demonstrate that the trust region method is superior to both the SA algorithm and SPGD algorithm with respect to convergence rates. These results indicate that the trust region method is a promising approach for correcting static or slowly changing wavefront aberrations in practical applications. © 2015 Optical Society of America

OCIS codes: (010.1080) Active or adaptive optics; (010.7350) Wave-front sensing.
http://dx.doi.org/10.1364/OL.40.001235

Static or dynamic aberrations can be corrected by the adaptive optics (AO) technique. In a traditional AO closed-loop control procedure, a wavefront sensor (WFS) is used to directly measure instantaneous wavefront aberrations. Based on the computed wavefront information, the corresponding correction that is deduced using a proper control algorithm can be implemented by the active correction elements.

In contrast to these common AO systems, some wavefront sensorless (WFSless) AO systems have emerged that do not need a WFS to measure the wavefront aberrations. Instead, they use the sensor signal that is nonlinearly related to the wavefront aberrations as feedback parameters for the correction elements. By adapting the correction elements, the aberration is corrected to maximize the image sharpness metric. Image sharpness is a measurement of the image performance and, in general, higher sharpness indicates better image quality.

The inherent nonlinear and nonderivative characteristics of the metric function make it difficult to solve the WFSless AO technique. There is no direct solution to the reflection relationship between the correction elements and the metric function. Iterative optimization algorithms are essential to solving these problems. Various optimization algorithms have been developed over the past decades. Gradient descent optimization methods such as stochastic parallel gradient descent (SPGD) have attracted much attention in the last decade [1]. In addition to SPGD, simulated annealing (SA) was proposed to correct aberrations for WFSless AO systems [2]. A well-known stochastic optimization algorithm, the real encoding genetic algorithm, has also been adopted to solve WFSless AO aberration correction [3].

In a common closed-loop WFSless AO system, the control objective is to maximize the image sharpness metric $f(k) \in \mathbb{R}$ at time k by adapting the deformable mirror (DM) actuator commands $u(k) \in \mathbb{R}^N$, i.e., $\max_{u(k)} f(k)$. As described in [4], it is assumed that the aberration can be corrected within a short time and by only a static nonlinearity intensity measurement. Moreover, if using a finite low-order Zernike aberration x to present the wavefront aberration, the system can be simplified as

$$f(k) \approx g(x + u(k)) + w(k), \tag{1}$$

where g represents an unknown static nonlinear wavefront-intensity mapping and $w(k)$ is the measurement noise. Therefore, the goal is to maximize $f(k)$ in a black-box fashion. The above equation considers the aberration as a disturbance directly applied to the input $u(k)$, which allows us to identify the model of the WFSless AO system based only on $u(k)$ and $f(k)$, and accounting for the influence of the aberration.

In the image-plane, the image sharpness metric can be given by $S_1 = \int \mathrm{d}x\mathrm{d}y I^2(x, y)$ [5]. Because it is difficult to obtain an accurate model of the above equation, there is no direct-form solution. Fortunately, a family of techniques called derivative-free methods can be adopted to tackle this black-box problem [6].

The quadratic approximation trust region method for derivative-free optimization (TRDF) [7] is adopted in this Letter. Studies have shown that TRDF is the most efficient way to solve medium-scale derivative-free problems [8].

TRDF uses $m = \frac{(n+1)(n+2)}{2}$ points of function $f(x)$ to construct a quadratic function, solving the original problem by progressively solving the quadratic optimization sub-problem. Two trust region radii ρ and Δ are defined in TRDF, where ρ is monotonically nonincreasing and controls the distances among the m interpolation points. An initial ρ_{beg} is assigned to ρ until it descends to a specified ρ_{end}. Radius Δ is used to control the range of new points.

We denote the m interpolation points as $x_i (i = 1, \ldots, m)$ at the beginning of each iteration, and x_k is the point that minimizes the function $f(x)$ among all the m points. By solving the sub-problem

$$\min_{d \in \Re^n} Q(x_k + d) \text{s.t.} \|d\|_2 \le \Delta, \tag{2}$$

we obtain a probe point, where $Q(x) = c_Q + g_Q^T(x - x_b) + \frac{1}{2}(x - x_b)^T G_Q(x - x_b)$ is a quadratic approximation of $f(x)$, $\Delta > 0$ is the trust region radius, and x_b is the initial point specified by the user. When ρ shrinks, x_b is

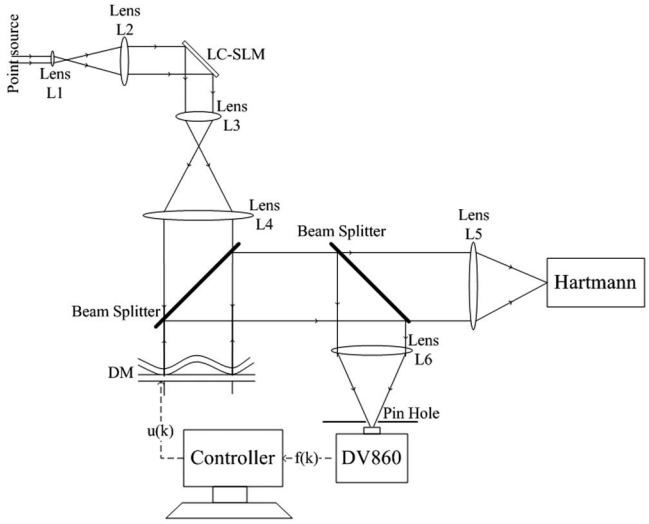

Fig. 1. Schematic of the experimental setup. The controller adapts the control signal $u(k)$ to maximize intensity measurement $f(k)$.

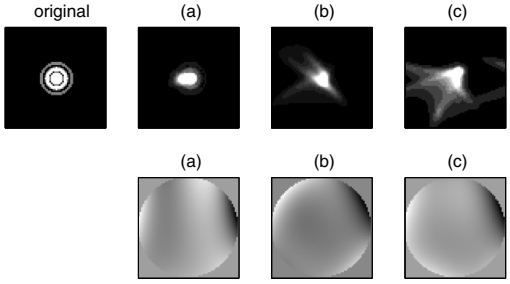

Fig. 2. Nondegraded images, various aberration-degraded images, and the aberration phase images.

substituted with the best point determined so far by TRDF. The values of c_Q, g_Q, and G_Q are determined by the interpolation conditions $Q(x_i) = f(x_i)$, $i = 1, \ldots, m$. In other words, for each $j = 1, 2, \ldots, m$, we derive a Lagrange interpolation function,

$$L_j(x) = c_j + g_j^T(x - x_b) + \frac{1}{2}(x - x_b)^T G_j(x - x_b), \quad (3)$$

and make

$$L_j(x_i) = \delta_{ij} = \begin{cases} 1, & \text{if } i = j, i = 1, \ldots, m \\ 0, & \text{if } i \neq j \end{cases}. \quad (4)$$

Obviously, $Q(x) = \sum_{j=1}^m f(x_j)L_j(x)$, and hence $c_Q = \sum_{j=1}^m f(x_j)c_j$, $g_Q = \sum_{j=1}^m f(x_j)g_j$, and $G_Q = \sum_{j=1}^m f(x_j)G_j$.

This framework minimizes $f(x)$ within a fixed accuracy and shrinks that accuracy gradually. For a fixed ρ, a new point $x_k + d$ is generated by m points using the quadratic function. If $f(x_k + d) < f(x_k)$, a better point has been reached. This better point replaces a certain point in $x_i (i = 1, \ldots, m)$ and the iteration continues. If $f(x_k + d) \geq f(x_k)$, Δ needs to shrink, and a new point is substituted with a worse interpolation point x_j to correct the model. This is called a model step. When solving the model step, the algorithm solves the following sub-problem:

$$\max_{d \in \Re^n} |L_j(x_k + d)| \text{s.t.} \|d\|_2 \leq \rho, \quad (5)$$

where index j corresponds to the moving interpolation point x_j.

To demonstrate the performance of the trust region method, the system was implemented experimentally using a He–Ne laser (wavelength 570 nm) as the point source and a liquid crystal spatial light modulator (LC-SLM) configured as a wavefront generator. The pupil diameter was set to 9 mm. An Andor DV860 with 2×2 binning mode at 900 Hz was used as an energy collector, which had an image size of 64×64 pixels. Static aberrations were adopted, and a 32 actuator DM was used to correct the aberration. To estimate the accuracy of the correction, we used a Hartmann to measure the residual wavefront aberration. Figure 1 shows the schematic of our experimental optical setup.

Considering the capacity of the DM, three different static aberration experiments were performed in this study. The first row in Fig. 2 shows the three images degraded by static aberration. The corresponding phase images are shown in the second row, respectively, and the approximate initial Zernike coefficients are listed in Table 1.

The two main parameters used in TRDF are Δ and ρ. Parameter ρ dominates the change of Δ in the iterations; thus, the actual parameter setting was for ρ. We set $\rho_{\text{beg}} = 0.1$ and $\rho_{\text{end}} = 10^{-6}$. This setting was fixed for all three procedures. We adopted Powell's method [9] to carry out our experiments.

The experimental results are listed in Fig. 3 and Table 2. From the first two images, we can see that the diffraction rings are reconstructed. Although the reconstruction degrades when the aberration increases, the energy is still concentrated.

Figure 4 presents the convergence rate and accuracy curve of TRDF. To demonstrate its performance, we compared TRDF with a bilateral SPGD and simplex SA [10]. The termination criterion was reached when the absolute difference between two adjacent function evaluations was less than 10^{-5} within 100 consecutive evaluations.

Table 1. Initial Zernike Coefficients[a]

Ex.	a_2	a_3	a_4	a_5	a_6	a_7	a_8	a_9	a_{10}	a_{11}	a_{12}
a	0	0	0.016	0	0.035	0.074	−0.062	0.011	−0.02	−0.038	0.016
b	0.3	0	0.41	0.2	0.14	0.046	−0.192	0.016	−0.12	−0.081	0.156
c	−1.0	0.2	0.35	0.1	0.32	0.24	−0.47	0.32	−0.21	−0.33	0.13

[a]The piston term is omitted.

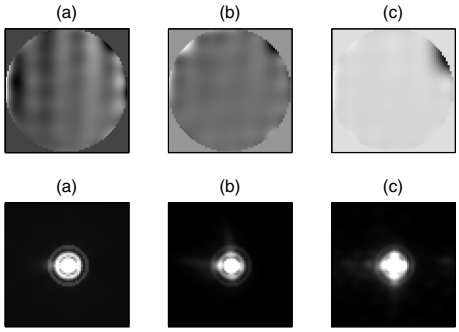

Fig. 3. Residual aberration phase images and the reconstructed images.

Table 2. Comparisons of the Initial Root Mean Square (rms) and Residual rms Wavefront Aberrations Calculated by TRDF, as Well as the Initial p-v and the Residual p-v Wavefront Aberrations Reached by TRDF

	rms λ		p-v λ	
Ex.	Initial	TRDF	Initial	TRDF
A	0.17556	0.0354	1.6308	0.3327
B	0.97084	0.23	8.617	2.7314
C	2.0739	1.0738	18.362	15.5126

The bilateral SPGD can be described as

$$u(k+1) = u(k) + \gamma \delta f(k) \delta u(k), \tag{6}$$

where $\delta f(k) = \delta f_+(k) - \delta J_-(k)$, $\delta f_+(k) = f(u(k) + \delta u(k)) - f(u(k))$, and $\delta f_-(k) = f(u(k) - \delta u(k)) - f(u(k))$. Furthermore, γ is the gain factor and $\delta u(k) = \{\delta u_1(k), \delta u_2(k), \ldots, \delta u_N(k)\}$ is the perturbed actuator command in the kth iteration. In addition, $\delta u_i(k)$ is independent and follows a Bernoulli distribution [11], i.e., the magnitude $|\delta u_i(k)| = \delta$ and $\Pr(\delta u_i(k) = \pm\delta) = 0.5$. In each iteration, bilateral SPGD requires three function evaluations, while both TRDF and SA require only one.

From Fig. 4 and Table 3, it is clear that TRDF has a similar Strehl ratio to SPGD and SA, while TRDF requires the lowest number of function evaluations to reach the maximum intensity. SPGD has the worst convergence rate in our experiments, but that may be caused by the parameter setting. Optimized parameter tuning could achieve better results. Simplex SA has a fast convergence rate because it uses a simplex method such as local search, as well as annealing to escape from local optima.

In conclusion, the trust region method is a local search algorithm. This deterministic algorithm can find the maximal energy of a WFSless AO system and has a fast convergence rate. Compared with the popular SPGD and SA algorithms, the trust region method is superior with respect to convergence rate when the scale of the DM is medium. We plan a series of continuous wavefront aberration experiments with white light or segmented mirrors in the near future.

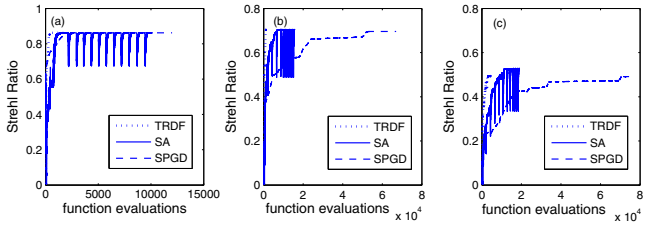

Fig. 4. Convergence rates of TRDF, SPGD, and SA for different aberrations. SPGD adopts (a) $\delta = 0.0001$, $\gamma = 3$, (b) $\delta = 0.0002$, $\gamma = 2$, and (c) $\delta = 0.0001$, $\gamma = 25$.

Table 3. Comparisons of the Strehl Ratio and Minimum Number of Function Evaluations Required to Achieve Stabilization

	Strehl Ratio		Stable Func. Eval.			
Ex.	TRDF	SA	SPGD	TRDF	SA	SPGD
a	0.8621	0.8624	0.8620	350	1100	1950
b	0.7049	0.7051	0.6959	1320	8470	59900
c	0.4941	0.5286	0.4979	4400	18670	79160

References

1. M. A. Vorontsov, G. W. Carhart, and J. C. Richlin, Opt. Lett. **22**, 907 (1997).
2. S. Zommer, E. N. Ribak, S. G. Lipson, and J. Adler, Opt. Lett. **31**, 939 (2006).
3. P. Yang, Y. Liu, M. Ao, S. Hu, and B. Xu, Opt. Laser Eng. **46**, 517 (2008).
4. H. Song, R. Fraanjie, G. Schitter, H. Kroese, G. Vdovin, and M. Verhaegen, Opt. Express **18**, 24070 (2010).
5. A. Buffington, F. S. Crawford, R. A. Muller, A. J. Schwemin, and R. G. Smits, J. Opt. Soc. Am. A **67**, 298 (1977).
6. A. R. Conn, K. Scheinberg, and L. N. Vicente, *Introduction to Derivative-Free Optimization*, MPS-SIAM Series on Optimization (SIAM, 2009).
7. M. J. D. Powell, Math. Program. **92**, 555 (2002).
8. L. M. Rios and N. V. Sahinidis, J. Global Optim. **56**, 1247 (2013).
9. "BOBYQA (Bound Optimization BY Quadratic Approximation)," http://mat.uc.pt/~zhang/software/bobyqa.zip.
10. "Java Simulated Annealing Package," http://sourceforge.net/projects/jannealer/.
11. J. C. Spall, IEEE Trans. Autom. Control **37**, 332 (1992).